Nonmodal analysis of helical and azimuthal magnetorotational instabilities

Magnetohydrodynamics 53(2017), 107-117

NONMODAL ANALYSIS OF HELICAL AND AZIMUTHAL MAGNETOROTATIONAL INSTABILITIES

G. Mamatsashvili[1,2,3], *F. Stefani*[1]

[1] *Helmholtz-Zentrum Dresden–Rossendorf, P.O. Box 510119, D-01314 Dresden, Germany*

[2] *Department of Physics, Faculty of Exact and Natural Sciences, Tbilisi State University, Tbilisi 0179, Georgia*

[3] *Abastumani Astrophysical Observatory, Ilia State University, Tbilisi 0162, Georgia*

Helical and azimuthal magnetorotational instabilities operate in rotating magnetized flows with relatively steep negative or extremely steep positive shear. The corresponding lower and upper Liu limits of the shear, which determine the threshold of modal growth of these instabilities, are continuously connected when some axial electrical current is allowed to pass through the rotating fluid. We investigate the nonmodal dynamics of these instabilities arising from the non-normality of shear flow in the local approximation, generalizing the results of the modal approach. It is demonstrated that moderate transient/nonmodal amplification of both types of magnetorotational instability occurs within the Liu limits, where the system is stable according to modal analysis. We show that for the helical magnetorotational instability this magnetohydrodynamic behavior is closely connected with the nonmodal growth of the underlying purely hydrodynamic problem.

Introduction. The helical and azimuthal magnetorotational instabilities are dissipation-induced instabilities that have attracted growing theoretical and experimental interest in recent years. They operate in magnetized shear flows with high resistivity, or very low magnetic Prandtl numbers, $\mathrm{Pm} = \nu/\eta \ll 1$, i.e. the ratio of viscosity ν to magnetic diffusivity $\eta = (\mu_0\sigma)^{-1}$. The helical magnetorotational instability (HMRI) was first discovered theoretically by Hollerbach & Rüdiger [1], who realized that adding an azimuthal field B_ϕ to a vertical field B_z can render a differentially rotating magnetized flow unstable even at very high resistivity up to the limit $\mathrm{Pm} = 0$, in contrast to the standard magnetorotational instability (SMRI) with a vertical magnetic field [2]. This property makes these instabilities amenable to experimental study in a Taylor-Couette (TC) setup filled with low $\mathrm{Pm} \sim 10^{-6} - 10^{-5}$ liquid metals. As a result, the first experimental detection of HMRI had followed shortly after its theoretical discovery [3]. HMRI was subsequently studied by means of linear modal stability analysis both with global TC (e.g., [4–6]) and local (short-wavelength) approaches (see e.g., [7–10] and references therein) as well as via experiments [11]. It was shown that HMRI is determined by the Reynolds number (Re) and by the Hartmann number (Ha), that ensures its persistence at high resistivity, where SMRI does not normally exist. Using the local analysis, Liu *et al.* [7] showed that in the presence of an imposed current-free azimuthal magnetic field HMRI operates for rotation profiles $\Omega(r)$ with negative or positive shear steeper than certain critical values. Specifically, these conditions expressed by the Rossby number $\mathrm{Ro} = r(2\Omega)^{-1}\mathrm{d}\Omega/\mathrm{d}r$ read as $\mathrm{Ro} < \mathrm{Ro}_{\mathrm{LLL}} = 2(1-\sqrt{2}) \approx -0.8284$ or $\mathrm{Ro} > \mathrm{Ro}_{\mathrm{ULL}} = 2(1+\sqrt{2}) \approx 4.8284$, where LLL and ULL refer to the lower and upper Liu limits, respectively.

The azimuthal magnetorotational instability (AMRI) is a non-axisymmetric relative of the axisymmetric HMRI that operates for dominant azimuthal field [12] and shares many properties with the latter. In particular, the same Liu limits

define the threshold of stability for AMRI too [10, 13]. The existence and importance of AMRI for steep positive shear was also shown recently [14, 15].

Apart from liquid metal flows in laboratory, low-Pm flows are found in a wide variety of astrophysical and geophysical settings: in the "dead zones" of protoplanetary disks, in stellar interiors and in the liquid cores of planets, which thus are the potential sites for HMRI and AMRI activity. Moreover, in compact objects like stars and planets, the condition of decreasing angular velocity (requirement for SMRI) is not everywhere met, for example, in the equator-near strip of the solar tachocline [16], which is also the region of sunspot activity [17].

The Liu limits imply that in the case of current-free field, HMRI and AMRI do not extend to the astrophysically important Keplerian rotation with $\mathrm{Ro}_{\mathrm{Kep.}} = -0.75$. To remedy the situation, Kirillov & Stefani [9] considered axial electrical currents not only at the axis, but also in the fluid, resulting in the azimuthal field $B_\phi(r)$ to deviate from the current-free profile $\propto 1/r$. They generalized the dispersion relation of Liu *et al.* [7] for this case and derived a new instability boundary – a curve in a plane that is spanned by Ro and a corresponding steepness of B_ϕ, called the magnetic Rossby number, $\mathrm{Rb} = r(2B_\phi/r)^{-1}\partial(B_\phi/r)/\partial r$. In the limit of large Re and Ha, this curve acquires the closed form

$$\mathrm{Rb} = -\frac{1}{8}\frac{(\mathrm{Ro}+2)^2}{\mathrm{Ro}+1}. \tag{1}$$

It is seen from this expression that the LLL and ULL are just the endpoints of this curve in the current-free regime $\mathrm{Rb} = -1$. Condition (1) indicates that even a small axial current within the liquid can break the lower Liu limit $\mathrm{Ro}_{\mathrm{LLL}}$ and enable HMRI and AMRI to operate for Keplerian profiles. This effect is now to be investigated in a planned liquid sodium TC experiment [18], which will combine and enhance the previous experiments on HMRI [11] and AMRI [19].

The above-mentioned linear studies of HMRI and AMRI were carried out in the framework of classical modal stability analysis of fluid mechanics, which focuses on the behavior at asymptotically large times. Instead, the nonmodal approach to the stability of shear flows focuses on the finite-time dynamics of perturbations, accounting for transient phenomena due to the shear-induced non-normality of the flow [20–22]. In this approach, one calculates the optimal initial perturbations that lead to the maximum possible linear amplification during some finite time. In self-adjoint flows, the perturbations that grow most are the least stable solutions of the modal eigenvalue problem. By contrast, in non-selfadjoint shear flows, the normal mode eigenfunctions are non-orthogonal due to the non-normality, resulting in transient, or nonmodal amplification of perturbations, often by factors much higher than that of the most unstable normal mode [21, 23]. So, leaving out the effects of the non-normality can give an incomplete picture of the overall dynamics (stability) of shear flows.

In this paper, we investigate the nonmodal dynamics of HMRI and AMRI in differentially rotating magnetized flows, which represent a special class of shear flows and hence the non-normality inevitably plays a role therein. Up to date, these instabilities have been studied using the modal approach. Recently, the nonmodal dynamics of SMRI was addressed by Squire & Bhattacharjee [23] and Mamatsashvili *et al.* [24]. Here we extend these investigations to the resistive, or low-Pm regime, where only HMRI and AMRI survive. One of our main goals is to link the magnetohydrodynamic features of these instabilities, including the universal two Liu limits derived with the modal approach, which still remain unexplained, to the nonmodal dynamics of perturbations in the hydrodynamic case.

1. Presentation of the problem. The main equations of non-ideal magnetohydrodynamics for incompressible conducting media are

$$\frac{\partial \mathbf{u}}{\partial t} + (\mathbf{u}\cdot\nabla)\mathbf{u} = -\frac{1}{\rho}\nabla\left(p + \frac{\mathbf{B}^2}{2\mu_0}\right) + \frac{(\mathbf{B}\cdot\nabla)\mathbf{B}}{\mu_0\rho} + \nu\nabla^2\mathbf{u}, \tag{2}$$

$$\frac{\partial \mathbf{B}}{\partial t} = \nabla\times(\mathbf{u}\times\mathbf{B}) + \eta\nabla^2\mathbf{B}, \tag{3}$$

$$\nabla\cdot\mathbf{u} = 0, \quad \nabla\cdot\mathbf{B} = 0, \tag{4}$$

where $\rho = const$ is the density, $\nu = \text{const}$ is the kinematic viscosity, and η is the magnetic diffusivity, p is the thermal pressure, $\mathbf{u}$ is the velocity and $\mathbf{B}$ is the magnetic field.

An equilibrium flow represents a fluid rotating with an angular velocity $\Omega(r)$ and threaded by a magnetic field, which comprises a constant axial component B_{0z} and an azimuthal one $B_{0\phi}$ with arbitrary radial dependence:

$$\mathbf{u}_0 = r\Omega(r)\mathbf{e}_\phi, \qquad \mathbf{B}_0 = B_{0\phi}(r)\mathbf{e}_\phi + B_{0z}\mathbf{e}_z.$$

Consider now small perturbations about this equilibrium, $\mathbf{u}' = \mathbf{u} - \mathbf{u}_0$, $p' = p - p_0$, $\mathbf{B}' = \mathbf{B} - \mathbf{B}_0$. Following [10], we adopt a local (Wentzel–Kramers–Brillouin (WKB)) approximation in the radial coordinate around some fiducial radius r_0, i.e. we assume perturbation length-scales to be much shorter than the characteristic length of radial variations of the equilibrium quantities, and represent the perturbations as $\mathbf{u}', \mathbf{B}' \propto \exp(\mathrm{i}k_r r + \mathrm{i}m\phi + \mathrm{i}k_z z)$, with azimuthal m, axial k_z and large radial k_r wavenumbers, $r_0 k_r \gg 1$ (without loss of generality we take $m, k_z > 0$). Linearizing Eqs. (2)– (4) about the equilibrium, introducing new variables $\xi = \mathrm{i}(k_z u'_\phi - m u'_z/r_0)$ and $\zeta = i(k_z B'_\phi - m B'_z/r_0)$ as in [23], and normalizing time by Ω^{-1}, distance by r_0 and velocity by $r_0\Omega$, we arrive at the following equations for the perturbations in the non-dimensional form (primes are omitted and the factor $(\mu_0\rho)^{-1/2}$ is absorbed in the magnetic field) [10, 23]

$$\frac{\mathrm{d}\boldsymbol{\psi}}{\mathrm{d}t} = \mathbf{A}\cdot\boldsymbol{\psi}, \tag{5}$$

where $\boldsymbol{\psi} \equiv (u_r, \xi, B_r, \zeta)$ is the state vector, and the evolution matrix operator $\mathbf{A}$ is

$$\mathbf{A} = \begin{pmatrix} -\frac{k^2}{\mathrm{Re}} + 4\mathrm{Ro}\frac{mk_r}{k^2} & -2\mathrm{i}\frac{\alpha}{k} & \mathrm{i}F & 2\mathrm{i}\omega_\phi\frac{\alpha}{k} \\ -2\mathrm{i}(1+\mathrm{Ro})k_z & -\frac{k^2}{\mathrm{Re}} & 2\mathrm{i}\omega_\phi(1+\mathrm{Rb})k_z & \mathrm{i}F \\ \mathrm{i}F & 0 & -\frac{k^2}{\mathrm{Rm}} & 0 \\ -2\mathrm{i}\omega_\phi\mathrm{Rb}\cdot k_z & \mathrm{i}F & 2\mathrm{i}\mathrm{Ro}\cdot k_z & -\frac{k^2}{\mathrm{Rm}}, \end{pmatrix}$$

where $k_r(t) = k_r(0) - 2\mathrm{Ro}\cdot mt$, $k^2 = k_r^2 + m^2 + k_z^2$, $\alpha = k_z/k$ and $F = m\omega_\phi + \omega_z$ with $\omega_\phi = B_{0\phi}/r_0\Omega$, $\omega_z = k_z B_{0z}/\Omega$. Note that for non-axisymmetric ($m \neq 0$) perturbations the radial wavenumber k_r varies with time due to the advection by the background flow and hence the matrix $\mathbf{A}$ also depends on time. The Reynolds number, $\mathrm{Re} = \Omega r_0^2/\nu$, and the magnetic Reynolds number, $\mathrm{Rm} = \Omega r_0^2/\eta$, are fixed to $\mathrm{Re} = 4000$ and $\mathrm{Rm} = 0.0056$, yielding a small magnetic Prandtl number $\mathrm{Pm} = \mathrm{Rm}/\mathrm{Re} = 1.4\cdot 10^{-6}$ typical for liquid metals. The strength of the imposed field is measured by the Hartmann number $\mathrm{Ha} = B_0 r_0/\sqrt{\nu\eta}$, which is in the range $\mathrm{Ha} \sim 10 - 100$ in liquid metal experiments [11, 19]. The relative effect of the azimuthal magnetic field to the axial one is characterized by the ratio $\beta = \omega_\phi/\omega_z$. The HMRI and AMRI are driven by the terms proportional to ω_ϕ in Eq. (5) and hence are effective in the presence of an appreciable azimuthal field, respectively,

for $\beta \sim 1$ and $\beta \gg 1$ (see, e.g., [7, 10]). We consider Rayleigh-stable rotation with $\mathrm{Ro} > -1$ and $\mathrm{Rb} < 0$, since the axial current decreases with radius. It is readily shown that $\mathbf{A}$ is indeed non-normal, i.e. it does not commute with its adjoint, $\mathbf{A}^\dagger \cdot \mathbf{A} \neq \mathbf{A} \cdot \mathbf{A}^\dagger$.

We quantify the nonmodal amplification in terms of the total perturbation energy, $E = \frac{\rho}{2}(|\mathbf{u}|^2 + |\mathbf{B}|^2) = \boldsymbol{\psi}^\dagger \cdot F^\dagger F \cdot \boldsymbol{\psi}$, where $\mathbf{F} = \sqrt{\rho/2} \cdot \mathrm{diag}(\alpha^{-1}, 1, \alpha^{-1}, 1)$, which is a physically relevant norm. The maximum possible, or optimal growth at a specific time t is defined as the ratio $G(t) = \max_{\boldsymbol{\psi}(0)} E(t)/E(0)$, where $E(t)$ is the energy at t and the maximization is done over all initial states $\boldsymbol{\psi}(0)$ with a given initial energy $E(0)$ (e.g., [21]). The final state at t is found from the initial state at $t = 0$ by solving the linear Eq. (5) and can be formally written as $\boldsymbol{\psi}(t) = \mathbf{K}(t) \cdot \boldsymbol{\psi}(0)$, where $\mathbf{K}(t)$ is the propagator matrix. Then, the maximum possible amplification $G(t)$ is usually calculated by the singular value decomposition of $\mathbf{K}$ at t (e.g., [21]). The square of the largest singular value gives the value of $G(t)$ and the corresponding initial condition that leads to this growth, the optimal perturbation is given by the right singular vector. We stress again that the nonmodal approach combined with the method of optimal perturbations is the most general way of analyzing shear flow dynamics (stability) at all times, as opposed to the modal approach, which is concerned only with the behavior at asymptotic times and hence omits important finite-time phenomena.

2. Dispersion relation. Before embarking on investigating the nonmodal dynamics of HMRI and AMRI, we briefly recap the results from the modal analysis of these instabilities in the local approach [6, 7, 10]. In this case, $|k_r(t)| \gg m$ or $k_z \gg m$ and, as a result, the shear-related term proportional to m in A_{11}, $4\mathrm{Ro} \cdot m k_r/k^2$, as well as the time-dependence of the radial and total wavenumbers are ignored, $\dot{k}_r(t)/|\mathrm{Ro}| \ll k_r(t)$, $\dot{k}(t)/|\mathrm{Ro}| \ll k(t)$. This admits the WKB approach in *time* when the solution can be sought in the form $\propto \exp(-\mathrm{i}\int \omega(t')dt')$, with the adiabatic condition $\dot{\omega}(t) \ll \omega^2(t)$ being fulfilled. Substituting this into Eq. (5) and taking the relevant limit of small magnetic Reynolds number, $\mathrm{Rm} \ll 1$ (inductionless approximation), but high Reynolds number, $\mathrm{Re} \to \infty$, we arrive at the following analytical expression for the growth rate $\gamma = Im(\omega)$ [10]

$$\gamma = (2\alpha^2\omega_\phi^2 \cdot \mathrm{Rb} - F^2)\frac{\mathrm{Rm}}{k^2} - \frac{k^2}{\mathrm{Re}} + \sqrt{2X + 2\sqrt{X^2 + Y^2}}, \tag{6}$$

where

$$X = \alpha^2\omega_\phi^2(\alpha^2\omega_\phi^2 \cdot \mathrm{Rb}^2 + F^2)\frac{\mathrm{Rm}^2}{k^4} - (\mathrm{Ro}+1)\alpha^2, \quad Y = \omega_\phi \alpha^2 F(\mathrm{Ro}+2)\frac{\mathrm{Rm}}{k^2}.$$

An instability occurs when $\gamma > 0$. Now consider the cases of HMRI and AMRI. HMRI relies on the growth of axisymmetric ($m = 0$) perturbations and appears from $\mathrm{Ha} \sim 10$. Taking the limit of small interaction parameter, $\mathrm{Ha}^2/\mathrm{Re} \ll 1$, and then maximizing with respect to β [$\beta \sim O(1)$], Eq. (6) simplifies to

$$\gamma = \alpha^2 \frac{\mathrm{Ha}^2}{\mathrm{Re}} \left[\frac{(\mathrm{Ro}+2)^2}{8(\mathrm{Ro}+1)(-\mathrm{Rb})} - 1\right], \tag{7}$$

(here Ha is defined in terms of B_{0z}, $\mathrm{Ha} = B_{0z}r_0/\sqrt{\nu\eta}$). On the other hand, AMRI consists in the growth of non-axisymmetric perturbations and takes place when the azimuthal magnetic field dominates over the axial one, corresponding to the limit $\beta \to \infty$ in Eq. (6),

$$\gamma = (2\alpha^2 \cdot \mathrm{Rb} - m^2)\frac{1}{k^2}\frac{\mathrm{Ha}^2}{\mathrm{Re}} - \frac{k^2}{\mathrm{Re}} + \sqrt{2X + 2\sqrt{X^2 + Y^2}}, \tag{8}$$

$$X = (\alpha^2 \cdot \mathrm{Rb}^2 + m^2)\frac{\alpha^2}{k^4}\frac{\mathrm{Ha}^4}{\mathrm{Re}^2} - (\mathrm{Ro}+1)\alpha^2, \quad Y = m(\mathrm{Ro}+2)\frac{\alpha^2}{k^2}\frac{\mathrm{Ha}^2}{\mathrm{Re}},$$

where now Ha is appropriately defined in terms of $B_{0\phi}$, $\mathrm{Ha} = B_{0\phi} r_0/\sqrt{\nu\eta}$. If the interaction parameter is small, $\mathrm{Ha}^2/\mathrm{Re} \ll 1$ and $\mathrm{Re} \to \infty$, Eq. (8) reduces to

$$\gamma = \frac{1}{k^2}\frac{\mathrm{Ha}^2}{\mathrm{Re}}\left(2\alpha^2 \cdot \mathrm{Rb} - m^2 + m\alpha\frac{\mathrm{Ro}+2}{\sqrt{\mathrm{Ro}+1}}\right). \tag{9}$$

To the leading order in Rm, the corresponding real part of the eigenfrequency is equal to the frequency of inertial waves (with the minus sign), $Re(\omega) = -\omega_{\mathrm{iw}} = -2\alpha\sqrt{1+\mathrm{Ro}}$. Remarkably, both Eqs. (7) and Eq. (9), after optimizing with respect to α, yield the same stability boundary (1) defined by $\gamma = 0$ [10], which indicates that for the current-free field $\mathrm{Rb} = -1$ the modal growth of HMRI and AMRI exists at negative shear less than the lower Liu limit $\mathrm{Ro} < \mathrm{Ro}_{\mathrm{LLL}} = -0.8284$ and at positive shear larger than the upper Liu limit $\mathrm{Ro} > \mathrm{Ro}_{\mathrm{ULL}} = 4.8284$, whereas at larger $\mathrm{Rb} > -1$ the stability region shrinks and the instability extends inside the Liu limits. So, the modal growth of HMRI and AMRI can, in principle, also exist for Keplerian rotation ($\mathrm{Ro}_{\mathrm{Kep.}} = -0.75$) starting from $\mathrm{Rb} = -0.781$ [9]. From Eq. (8) it follows that in these intervals of Rossby numbers, AMRI operates (i.e. $\gamma > 0$) only in a certain range of radial wavenumbers, outside this range $\gamma < 0$ and the perturbations decay due to resistivity. Since we are interested in the effects of non-normality on the dynamics of HMRI and AMRI, below we focus on the current-free azimuthal field, i.e. fix $\mathrm{Rb} = -1$, where free energy for instability comes solely from shear.

3. Nonmodal dynamics of HMRI. Now, following [25], we investigate the nonmodal growth of axisymmetric HMRI by solving an initial value problem given by Eq. (5), as described in Section 1, without restricting the time-dependence of harmonics (modes) to the exponential form, as accepted in modal analysis. In

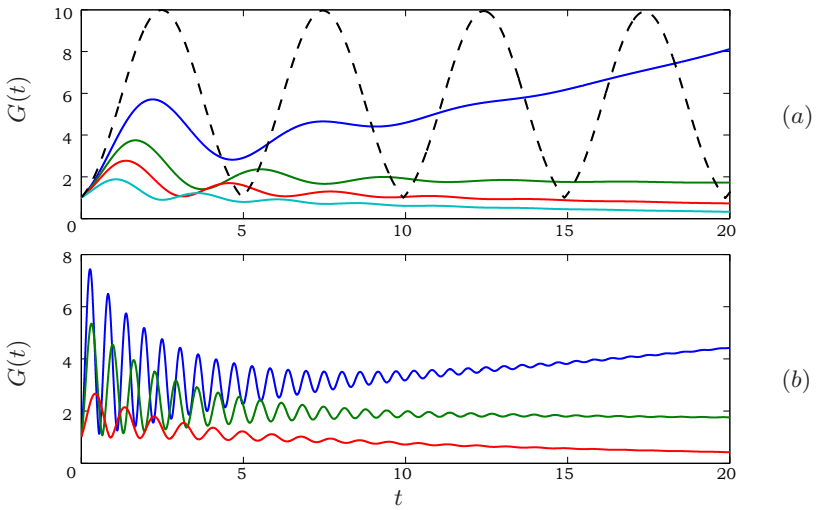

Fig. 1. $G(t)$ for HMRI with $m = 0$ at different (*a*) $\mathrm{Ro} = -0.9$ (blue), –0.8284 (LLL, green), –0.75 (Kepler, red), –0.6 (cyan) and (*b*) $\mathrm{Ro} = 2$ (red), 4.8284 (ULL, green), 7 (blue). For reference, the dashed black curve in panel (*a*) shows the maximum growth factor vs. the time in the nonmagnetic case at $\mathrm{Ro} = -0.9$. The other parameters are $\alpha = 1$ and $k = 1$. For each Ro, the parameter β is chosen such that to maximize the modal growth rate for other given parameters.

the case of axisymmetric HMRI, k_r does not vary with time and hence the evolution matrix $\mathbf{A}$ is stationary. Fig. 1 shows the maximum energy growth $G(t)$ at modally stable and unstable Ro together with the growth in the modally stable nonmagnetic case, where only the nonmodal growth is possible. For HMRI we take the Hartmann number Ha $=15$. In all cases, the initial stage of evolution is qualitatively similar: the energy increases with time, reaches a maximum G_m and then decreases. This first nonmodal amplification phase is followed by minor amplifications. Like in the case of modal growth, the kinetic energy dominates over the magnetic one also during the nonmodal growth. As a result, the duration of each amplification event is set by inertial waves: the peak value G_m is attained at around one quarter of the wave period, $t_\mathrm{m} \approx \pi/2\omega_\mathrm{iw}$, similar to that in the nonmagnetic case, although its value is smaller than that in the latter case. At larger times, the optimal growth follows the behavior of the modal solution – it increases (for Ro $= -0.9$, 7), stays constant (for the Liu limits, Ro $= \mathrm{Ro_{LLL}}, \mathrm{Ro_{ULL}}$) or decays (for Ro $= -0.75$, -0.6, 2), respectively, if the flow is modally unstable, neutral or stable; in the latter case HMRI undergoes only transient amplification. This is readily understood: at large times the least stable modal solution (with the growth rate given by Eq. 7) dominates, whereas at small and intermediate times the transient growth due the interference of non-orthogonal eigenfunctions is important. In particular, for the Liu limits, where the modal growth is absent, there is a moderate nonmodal growth $G_\mathrm{m}(\mathrm{Ro_{LLL}}) = 4.06, G_\mathrm{m}(\mathrm{Ro_{ULL}}) = 5.46$. A similar evolution of the axisymmetric perturbations' energy with the time for HMRI was already found in [5], where also the physical mechanism of HMRI was explained in terms of the additional coupling between meridional and azimuthal flow perturbations. Importantly, in Fig. 1, the G_m values at modally stable and unstable Rossby numbers are comparable and several times larger than the modal growth factors during the same time t_m. Indeed, for example, at Ro $= -0.9$ the growth achieves the first peak $G_\mathrm{m} = 5.71$ at $t_\mathrm{m} = 2.2$, while at this time the energy of the normal mode would have grown only by a factor of $\exp[2t_\mathrm{m}\gamma(\mathrm{Ro})] = 1.135$. This also implies that in the Keplerian regime, where there is no modal growth of HMRI for Rb $= -1$, we still observe a moderate nonmodal growth (red curve in Fig. 1*a*).

Fig. 2, which is the central result of this paper, shows (*a*) the maximum growth G_m in the magnetic and nonmagnetic cases as well as (*b*) the modal growth rate γ given by Eq. (7) versus Ro. G_m increases linearly with Ro at Ro > 0 and much steeper at Ro < 0 which can be well approximated by $\propto (1 + \mathrm{Ro})^{-0.78}$. For comparison, in this plot we also show the maximum transient growth factor for axisymmetric perturbations in the nonmagnetic case, $G_\mathrm{m}^{(h)} = (1+\mathrm{Ro})^{\mathrm{sgn(Ro)}}$, from [26]. So, although G_m in the magnetic case is slightly smaller than that in the nonmagnetic one, the two curves are in fact close to each other and display nearly the same dependence on Ro. Note that the dependences of G_m, $G_\mathrm{m}^{(h)}$ (Fig. 2*a*) and of the modal growth rate γ (Fig. 2*b*) on Ro have very similar shapes. Remarkably, the latter, being given by Eq. (7), can be expressed in terms of the hydrodynamic nonmodal growth $G_\mathrm{m}^{(h)} = (1 + \mathrm{Ro})^{\mathrm{sgn(Ro)}}$ in the closed form

$$\gamma = \alpha^2 \frac{\mathrm{Ha}^2}{\mathrm{Re}} \left[\frac{(G_\mathrm{m}^{(h)} + 1)^2}{8 G_\mathrm{m}^{(h)}} - 1 \right], \tag{10}$$

which is indeed proportional to $G_\mathrm{m}^{(h)}$ for larger values. Both Liu limits are, therefore, connected with a corresponding threshold

$$G_\mathrm{m}^{(h)}(\mathrm{Ro_{LLL}}) = G_\mathrm{m}^{(h)}(\mathrm{Ro_{ULL}}) = 5.828.$$

4. Nonmodal dynamics of AMRI. For non-axisymmetric AMRI, the radial wavenumber changes with time due to background shear and, as a result, its dynamics differs from that of axisymmetric HMRI. The adiabatic WKB regime in time applies only at $|k_r(t)| \gg m$ ($k_z \lesssim m$), then $|k_r|$ decreases with time and

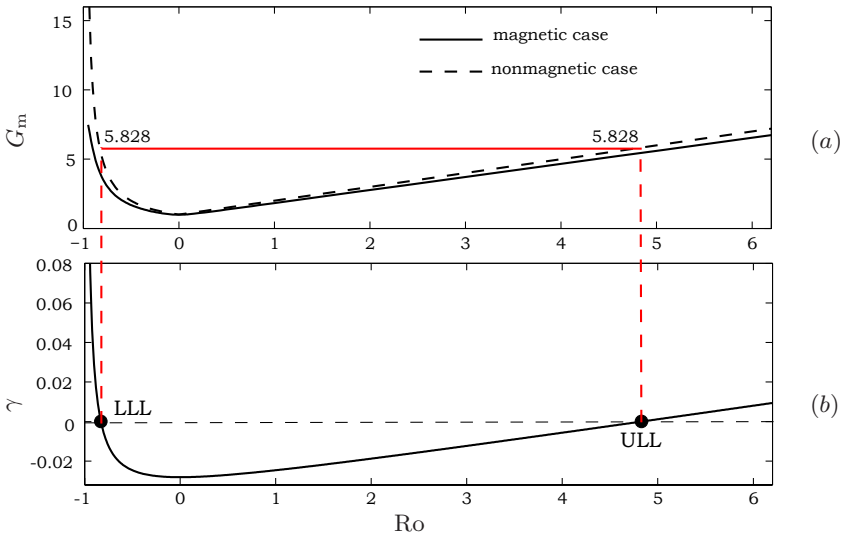

Fig. 2. Shown are (*a*) G_m for HMRI (solid line) and for the nonmagnetic case (dashed line) as well as (*b*) the modal growth rate of HMRI from Eq. (7) vs. Ro. Other parameters are as in Fig. 1. Red lines illustrate the connection between the Liu limits of HMRI and the nonmodal growth in the purely hydrodynamic case.

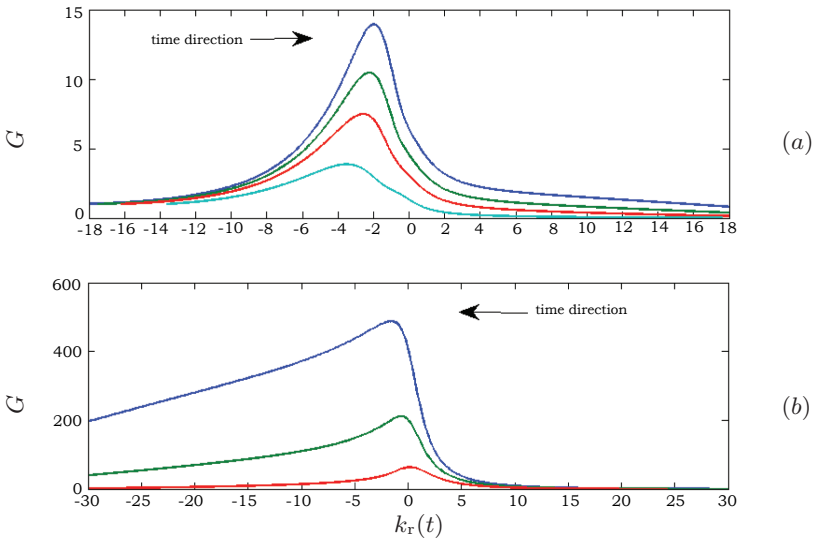

Fig. 3. $G(t)$ as a function of the time-dependent $k_r(t)$ for AMRI with $m = 1$ and $k_z = 1$ at different negative Rossby numbers (*a*) Ro = −0.9 (blue), –0.8283 (LLL, green), –0.75 (Keplerian, red), –0.6 (cyan), when k_r increases with time from negative to positive values, and at positive Rossby numbers (*b*) Ro = 3 (red), 4.8284 (ULL, green), 7 (blue), when k_r decreases with time from positive to negative values. Each curve has been maximized with respect to the initial value of the radial wavenumber $k_r(0)$. The growth is higher the larger is shear |Ro|.

enters the non-adiabatic interval in the neighborhood of $|k_r(t)| \sim m$, where the dispersion relation (8) and hence the modal approach are no longer applicable for the description of AMRI. In this case, one should resort to numerical integration of Eq. (5) to study the dynamics of perturbations and quantify their nonmodal amplification. It is in this non-adiabatic region, where the effects of non-normality manifest themselves and influence the dynamics of AMRI. Obviously, the modes with such initial $k_r(0)$ that do not lead to crossing the non-adiabatic interval, i.e. with $k_r(0)$ and $\mathrm{Ro} \cdot m$ having opposite signs, do not experience the transient growth and decay quickly due to resistivity. Here, we restrict ourselves to the most amplified $m = 1$ modes, whereas the dynamics of other modes with larger m which usually grow less than the $m = 1$ modes do, will be presented elsewhere. Fig. 3 shows the evolution of the maximum energy growth $G(t)$ for these harmonics at various Ro, including the Keplerian rotation, and fixed $k_z = m = 1$. The function G has been maximized over the initial wavenumber $k_r(0)$, which is negative (positive) at $\mathrm{Ro} < 0$ ($\mathrm{Ro} > 0$) and $|k_r(0)| \gg m$. The Hartmann number characterizing the azimuthal field is set to $\mathrm{Ha} = 100$, which is typical for AMRI [19]. Initially, in the adiabatic region, the effect of resistivity on the mode is still appreciable. As the mode evolves, $|k_r(t)|$ decreases with absolute value, the resistive dissipation becomes weaker, whereas the effect of nonnormlity/shear gets stronger. As a result, the energy starts to amplify, extracting energy from the background flow. Then, $|k_r(t)|$ enters the non-adiabatic region, where the effect of non-normality is largest. As a consequence, G exhibits most of growth just in this interval of radial wavenumbers, reaching a maximum G_m at different $|k_{r,m}| \lesssim 3$, which depend on Ro, but are close to each other. The peak G_m is higher the larger is the shear $|\mathrm{Ro}|$ (see also Fig. 4). Afterwards, $|k_r|$ increases again, leaving the non-adiabatic area, and the harmonic's energy gradually decreases and eventually decays due to viscosity and resistivity at high enough k_r. We refer to the whole process as the nonmodal growth of AMRI, which always lasts for a finite time in the local approach because of the shear-induced time variation of the radial wavenumber of non-axisymmetric modes. Note that like in the case of HMRI, the moderate nonmodal growth occurs also at the Liu limits and Keplerian rotation, which are, respectively, marginally stable and fully stable according to modal analysis.

As mentioned above, the optimal perturbation and optimal growth formalism that we use here, as opposed to the modal approach, is the most general way to describe the dynamics of non-axisymmetric perturbations both in nonmodal and modal regimes. In the adiabatic regime, for HMRI, it gives the results of the modal analysis, whereas for AMRI, one should additionally take into account the time-dependence of the radial wavenumber, but neglect the shear-induced terms in Eq. (5) (the second term in A_{11}), which are small in this regime. The situation in this highly resistive flow is analogous to the nonmodal (transient) growth of non-axisymmetric perturbations in modally/spectrally stable unmagnetized shear flows [27, 28], except that with the imposed azimuthal magnetic field there exists an additional means of energy gain from the mean flow due to the terms proportional to ω_ϕ in main Eq. (5) that are responsible for AMRI, whose dynamics itself is modified by the non-normality. By contrast, for axisymmetric perturbations (i.e. for HMRI), as seen above, the nonmodal amplification precedes the modal growth, which is dominant at large times.

Fig. 4 shows the dependence of G_m on the axial wavenumber k_z at several (a) negative and (b) positive Rossby numbers. At larger absolute values of Ro, i.e. for $\mathrm{Ro} = -0.92$, –0.9 and 7, it first increases with k_z, achieving a peak at $k_{z,m} \sim 1 - 2$, and then decreases at large k_z, more rapidly for positive shear. The critical wavenumber $k^{z,m}$ decreases with $|\mathrm{Ro}|$ and eventually becomes $k^{z,m} = 0$.

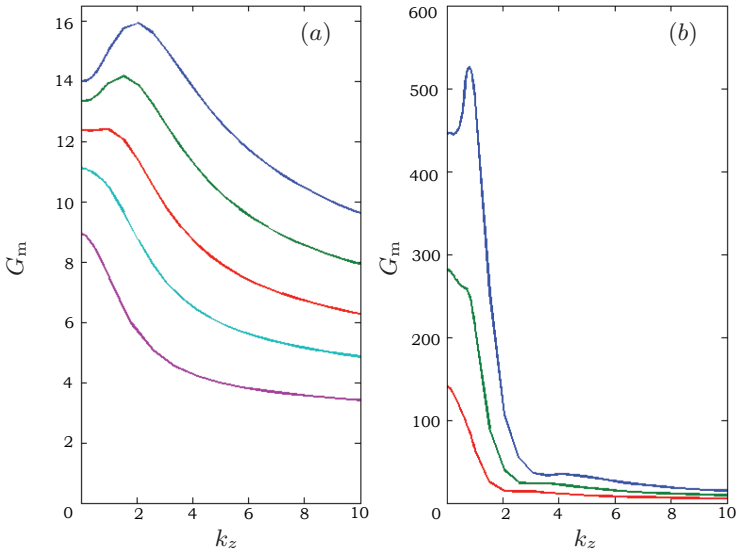

Fig. 4. G_m vs. k_z for the $m = 1$ modes at various Rossby numbers (*a*) Ro $= -0.92$ (blue), –0.9 (green), -0.87 (red), –0.8284 (LLL, cyan) –0.75 (Kepler, violet) and (*b*) Ro $= 3$ (red), 4.8284 (ULL, green), 7 (blue). For positive shear (*b*), the nonmodal growth is more than an order of magnitude larger than for negative one.

As seen in Fig. 4, the nonmodal growth is more than an order of magnitude larger at positive Ro than at negative Ro, indicating the importance of positive shear for AMRI, as was already shown recently in [14] using the modal approach. Note that $k_{z,m} \sim m$ falls in the non-adiabatic regime, implying that the nonmodal approach is more appropriate to describe the dynamics of AMRI rather than modal one at these axial wavenumbers that yield the maximum growth. At $k_z \gg m$, the temporal WKB approximation holds at all times during the evolution (except near the points $\gamma(k_r) = 0$, if any). Due to our general treatment of the initial value problem posed by Eq. (5), the growth factor at large k_z in Fig. 4 essentially coincides with that given by modal analysis.

5. Conclusions. In this paper, we investigated the linear nonmodal dynamics of HMRI and AMRI due to the non-normality of shear magnetized flow with large resistivity in the local approximation. As a main tool of analysis, we used the nonmodal approach in combination with the optimal perturbation formalism, which allows to characterize the growth of perturbations in most general form, comprising the modal regime. We traced the entire time evolution of modes by solving an initial value problem, thereby capturing the finite-time nonmodal dynamics. As shown in Fig. 2 and quantified exactly in Eq. (10), the modal growth rate of HMRI exhibits a very similar dependence on Ro as the maximum nonmodal growth in the purely hydrodynamic shear flow, establishing a fundamental link between the nonmodal dynamics and the dissipation-induced modal instabilities, such as HMRI. Despite the latter being of magnetic origin, both rely on the hydrodynamic means of amplification, i.e. extract energy from the background flow mainly by Reynolds stress due to shear/non-normality [5]. The dynamics of AMRI is more complex due to the shear-induced time-variation of the radial wavenumber of non-axisymmetric modes. As a result, in the local approach, the growth of AMRI both in modal (adiabatic) and nonmodal (non-adiabatic) regimes is always transient. The maximum nonmodal growth factor increases with shear,

i.e. with the absolute value of the Rossby number and achieves an order of magnitude higher values at positive shear than at negative shear, consistent with the recent findings of [14] on the existence and importance of AMRI for positive shear.

Acknowledgements. This work was supported by the Alexander von Humboldt Foundation and by the Helmholtz Association in framework of the Helmholtz Alliance LIMTECH. Discussions with M. Avila and A. Guseva are gratefully acknowledged.

References

[1] R. Hollerbach, G. Rüdiger. *Phys. Rev. Lett.*, vol. 95 (2005), art. no. 124501.

[2] S.A. Balbus, J.F. Hawley. *Rev. Mod. Phys.*, vol. 70 (1998), p. 1.

[3] F. Stefani *et al.* *Phys. Rev. Lett.* vol. 97 (2006), art. no. 184502.

[4] G. Rüdiger, M. Schultz. *Astron. Nachrichten,* vol. 329 (2008), p. 659.

[5] J. Priede, I. Grants, G. Gerbeth. *Phys. Rev. E*, vol. 75 (2007), art. no. 047303.

[6] J. Priede. *Phys. Rev. E*, vol. 84 (2011), art. no. 066314.

[7] W. Liu, J. Goodman, I. Herron, H. Ji. *Phys. Rev. E,* vol. 74 (2006), art. no. 056302.

[8] O. Kirillov, F. Stefani. Astrophys. J., vol. 712 (2010), p. 52.

[9] O. Kirillov, F. Stefani. *Phys. Rev. Lett.*, vol. 111 (2013), art. no. 061103.

[10] O. Kirillov, F. Stefani, Y. Fukumoto. *J. Fluid Mech.*, vol. 760, (2014), p. 591.

[11] F. Stefani *et al.* *Phys. Rev. E*, vol. 80, (2009) , art. no. 066303.

[12] R. Hollerbach, V. Teeluck, G. Rüdiger. *Phys. Rev. Lett.*, vol. 104 (2010), art. no. 044502.

[13] O. Kirillov, F. Stefani, Y. Fukumoto. *Astrophys. J.,* vol. 756 (2012), p. 83.

[14] F. Stefani, O. Kirillov. *Phys. Rev. E*, vol. 92 (2015), art. no. 051001.

[15] G. Rüdiger et al. *Phys. Fluids* vol. 28 (2016), art. no. 014105.

[16] K.P. Parfrey, K. Menou. *Astrophys. J. Lett.,* vol. 667 (2007), p. L207.

[17] P. Charbonneau. *Liv. Rev. Sol. Phys.* vol. 7 (2010), p. 3.

[18] F. Stefani *et al.* *Magnetohydrodynamics,* vol. 48 (2012), no. 1, p. 103–113.

[19] M. Seilmayer *et al.* *Phys. Rev. Lett.*, vol. 113, (2014), art. no. 024505.

[20] L. Trefethen, A. Trefethen, S. Reddy, T. Driscoll. *Science,* vol. 261 (1993), p. 578,

[21] P. Schmid, D. Henningson. *Stability and Transition in Shear Flows.* (Springer Verlag, New York, 2001.)

[22] P. Schmid. *Annu. Rev. Fluid Mech.,* vol. 39 (2007), p. 129.

[23] J. Squire, A. Bhattacharjee. *Phys. Rev. Lett.,* vol. 113 (2014), art. no. 025006.

[24] G. Mamatsashvili *et al.* *Mon. Not. R. Astron. Soc.,* vol. 435 (2013), p. 2552.

[25] G. Mamatsashvili, F. Stefani. *Phys. Rev. E*, vol. 94 (2016), art. no. 051203.

[26] N. Afshordi, P. Mukhopadhyay, R. Narayan. *Astrophys. J.,* vol. 629 (2005), p. 373.

[27] B. Mukhopadhyay, N. Afshordi, R. Narayan. *Astrophys. J.,* vol. 629 (2005), p. 383.

[28] S. Maretzke, B. Hof, M. Avila. *J. Fluid Mech.,* vol. 742, (2014), p. 254.